EAI Endorsed Transactions
on Energy Web

Research Article EAI.EU

Consistency Monitoring of Wind Turbine Blade Loads Based on MEMS Optical Fiber Sensing

Yong Xue[1], Yang Li[1], Xiangye Fan[1], Binshan Xie[1], Zhiyuan Ma[2,3], Lin Lin[2,3], Mengnan Cao[2,3]*

[1]State Power Investment Group Xinjiang Energy and Chemical Emin Co., Ltd., Tacheng City, Xinjiang,834035, China
[2]Shanghai Power Equipment Research Institute CO, LTD, Shanghai, 201625, China
[3]SPIC Energy Science and Technology Research Institute,shanghai, 201625, China

Abstract

INTRODUCTION: This paper presents a comprehensive structural monitoring framework for wind turbine blades based on MEMS-FBG (micro-electro-mechanical systems—fiber Bragg grating) sensor fusion technology.
OBJECTIVES: The system integrates high-resolution strain and vibration sensing across multiple blade segments, combined with real-time data processing, fault detection, and SCADA-level visualization.
METHODS: A multilayered load consistency model is introduced, incorporating thermal compensation, strain-to-load calibration, and a novel consistency index (η) to quantify inter-blade aerodynamic symmetry.
RESULTS: Experimental validation was conducted on a 2.0 MW wind turbine over a 60-day continuous monitoring campaign. Static calibration demonstrated a load reconstruction accuracy within ±3%, while dynamic data revealed a strong correlation between load and blade vibration ($R \geq 0.86$).
CONCLUSION: Fault simulation through pitch angle manipulation confirmed the system's rapid alarm response within 3 seconds for major asymmetry events. Additionally, signal drift testing showed MEMS-FBG sensors exhibited 80–95% lower drift than conventional resistance strain gauges under rotating and EMI-intensive conditions.

Keywords: MEMS-FBG Sensors; Wind Turbine Blade Monitoring; Load Consistency Index; Strain-to-Load Calibration; SCADA Integration; Signal Drift Analysis; Anomaly Detection.

Received on 23 May 2025, accepted on 23 September 2025, published on 14 October

doi: 10.4108/ew.9387

*Corresponding author. Email: mengnam_cao987@outlook.com

1. Introduction

This is the body text with no indent. The global transition toward renewable energy has become a pressing priority in response to the dual challenges of environmental sustainability and energy security. Wind power, as one of the most mature and rapidly expanding forms of clean energy, plays a pivotal role in this transition[1]. Central to wind energy systems are the turbine blades, which are subjected to complex and fluctuating loads during operation. These include aerodynamic forces, gravitational loads, centrifugal forces, and vibrational stresses, all of which may vary with wind speed, yaw angle, turbulence, and blade pitch. Over time, these variable loads can lead to fatigue, structural degradation, or even catastrophic failure[2,3]. Therefore, monitoring the mechanical. Behaviour and load consistency of wind turbine blades in real time are essential for ensuring operational safety, extending service life, and optimising energy output.

Traditionally, structural health monitoring (SHM) of wind turbine blades has relied on techniques such as resistance strain gauges, piezoelectric sensors, acoustic emission testing, ultrasonic inspection, and infrared thermography [4, 5]. While these methods offer varying degrees of sensitivity and precision, they suffer from inherent limitations. Resistance-based sensors are prone to drift and require frequent recalibration to maintain accuracy. Ultrasonic and acoustic systems are vulnerable to environmental noise and require complex signal processing. Moreover, most conventional sensors are susceptible to electromagnetic interference, have limited durability in harsh weather conditions, and are difficult to

Integrate into the rotating components of wind turbines. In addition, these methods often rely on discrete point measurements and fail to provide comprehensive spatial coverage or real-time inter-blade comparisons, making it difficult to detect subtle asymmetries or early-stage faults [6].

MEMS-FBG sensors provide a reliable and advanced solution for monitoring wind turbine blades. They combine high sensitivity with excellent signal stability and resistance to electromagnetic interference. Compared to piezoelectric and acoustic sensors, MEMS-FBGs are more consistent and less affected by environmental noise. Unlike ultrasonic and infrared methods, they support real-time, continuous monitoring. Optical interferometers and wireless networks, although sensitive and flexible, face challenges such as complexity and power limitations. MEMS-FBG sensors enable accurate, distributed sensing along the blade. Their compact, embedded design makes them ideal for long-term structural health monitoring in harsh turbine environments.

To overcome these challenges, researchers and engineers have increasingly turned to optical fibre sensing technologies, particularly those based on fibre Bragg grating (FBG) and micro-electro-mechanical systems (MEMS). FBG sensors operate by reflecting specific wavelengths of light, which shift in response to mechanical strain or temperature changes[7,8]. When combined with MEMS structures, these sensors form compact, low-power, and highly sensitive systems capable of precise measurement over long distances. MEMS-FBG sensors offer several critical advantages, including immunity to electromagnetic interference, corrosion resistance, a high signal-to-noise ratio, and multiplexing capability, which allows multiple sensors to share a single fibre optic line. Additionally, their small size and flexibility make them ideal for embedding directly into the composite materials of turbine blades without compromising structural integrity [9,10]. MEMS-FBG sensors offer major benefits over traditional sensors for structural health monitoring. They are electromagnetic interference-free, allowing for precise and stable measurements in noisy environments, such as those found in wind turbines. This results in low signal drift compared to conventional resistance strain gauges. They are multiplexed, which eliminates wiring complexity and enables distributed sensing by allowing multiple sensors to be accommodated on a single optical fibre. MEMS-FBG sensors are robust against severe weather, small, and corrosion-free. Grandhi inspired the energy-efficient integration of renewable systems with environmental sustainability. Our research incorporates this approach in designing a low-power, HMI-integrated passive IoT optical fibre sensor network for real-time water level monitoring, enabling autonomous operation, clean technology deployment, and improved efficiency in remote environments [11].

MEMS-FBG sensors offer significant advantages over conventional resistance strain gauges in wind turbine blade monitoring, providing highly accurate readings with minimal signal drift, thereby ensuring long-term consistency of performance. The immunity to electromagnetic interference enhances signal stability in interference-prone environments. The sensors are also resistant to corrosion and harsh weather conditions. They are compact and easy to integrate into the blade structure. They also facilitate distributed sensing, making real-time monitoring along the entire length of the blade possible.

Recent developments in both academia and industry have highlighted the potential of MEMS-FBG sensors for wind turbine applications. For instance, several European manufacturers, including Vestas and Siemens Gamesa, have piloted optical fiber-based monitoring systems in commercial turbines. In South Korea, researchers have demonstrated the feasibility of using FBG sensors for real-time load and vibration detection in experimental blades [12]. China, too, has made significant progress in the localization of MEMS-FBG sensor fabrication and system integration. However, despite these advancements, existing research and commercial products rarely address the need for **inter-blade load consistency monitoring**—the comparative analysis of dynamic loads across multiple blades, which is vital for identifying structural asymmetry, pitch deviation, or rotor imbalance in real time [13,14]. Wind turbine unbalanced loads lead to higher wear, vibrations, and potential structural damage, lowering efficiency and reliability. Such occurrences are a result of uneven stress on the blade and drivetrain parts, resulting in quicker fatigue and possible damage. MEMS FBG sensors enable the real-time detection of such imbalances by precise strain and vibration measurement. Their excellent stability and minimal signal drift make them suitable for continuous monitoring, enabling timely fault detection and improved turbine performance.

Recognising this gap, the present study proposes a comprehensive MEMS-FBG optical fibre sensing system specifically designed for multi-blade, real-time load consistency monitoring in utility-scale wind turbines. The system enables distributed sensing along each blade, supports high-frequency data acquisition, and integrates seamlessly with turbine SCADA (Supervisory Control and Data Acquisition) systems for remote monitoring and control. In this paper, we detail the architectural design of the sensing network, present the mathematical modelling framework for load calculation and consistency evaluation, and validate the system through experimental deployment on full-scale wind turbines. We also introduce a set of derived indicators—including load balance coefficient, correlation with blade vibration, and consistency index—to quantify structural integrity over time. Our results demonstrate the system's ability to detect load asymmetries, correlate structural loads with dynamic behavior, and identify early signs of fatigue or fault conditions [15]. The MEMS-FBG technology integrates microelectromechanical systems (MEMS) with fibre Bragg grating (FBG) optical sensors to deliver accurate, real-time readings of strain, temperature, and vibration. These sensors possess high sensitivity, are immune to electromagnetic interference, and are appropriate for direct use.

Integration into turbine blades. To assess the distribution of mechanical loads on blades, the system presents the load consistency index (η), a statistical measure that gauges the evenness of blade loading. Higher values signify improved aerodynamic symmetry and structural equilibrium. Moreover, the system includes complete SCADA integration, allowing real-time data from the sensors to be processed and displayed via the turbine's Supervisory Control and Data Acquisition platform. Kumar et al. emphasised optimising wind and solar energy performance with a focus on environmental sustainability. Their technique is adopted in our proposed work through MEMS-based optical fiber sensing to monitor wind turbine blade loads. This enhances turbine reliability and more stable renewable energy generation [16]. The renewable energy domain enables real-time monitoring of wind turbine blade loads using MEMS optical fibre sensing. The high-frequency data captured offers a strong foundation for applying deep learning techniques to predict structural behavior, detect anomalies, and enhance maintenance strategies. Although the primary focus is on sensing technology, the approach supports integration with deep learning models such as LSTMs or autoencoders for time-series analysis and anomaly detection.

This work contributes to the field of wind energy monitoring by providing a scalable and reliable methodology for continuous blade load assessment, which supports predictive maintenance strategies and enhances turbine reliability. The remainder of the paper is structured as follows: Section 2 introduces the overall system design, sensor calibration methods, and signal interpretation models. Section 3 presents the field deployment, experimental procedures, and data analysis. Section 4 concludes with a summary of findings and directions for future research and engineering implementation.

2. System Design and Implementation Scheme

This section provides a comprehensive overview of the hardware architecture, sensor selection, data processing methodology, and communication protocols employed in the MEMS-FBG-based wind turbine blade load monitoring system. The system is designed to capture distributed strain, vibration, and temperature data from multiple blades and convert these into interpretable load consistency metrics in real time [17,18].

2.1 Sensing Architecture and System Overview

The system architecture consists of MEMS-FBG strain sensors, MEMS accelerometers, optical fiber cables, wavelength demodulation units, a n d industrial control processors, and a SCADA-connected data visualization platform. Sensors are embedded directly into the blade structure or mounted near critical cross-sections. Each blade is equipped with 8 strain sensors and 3 accelerometers. Correct mounting of MEMS-FBG sensors on wind turbine blades requires proper surface preparation, high epoxy bonding, cured control, and protection. Surfaces are cleaned and ground before application of high-strength adhesives, with curing either at room temperature or accelerated through heat. Sensors are encapsulated by shielding and coating after curing to protect them from moisture, extreme temperatures, and vibration. Strain relief and correct routing of optical fibres add further durability. These processes ensure the long-term stability and performance of sensors in demanding operating conditions.

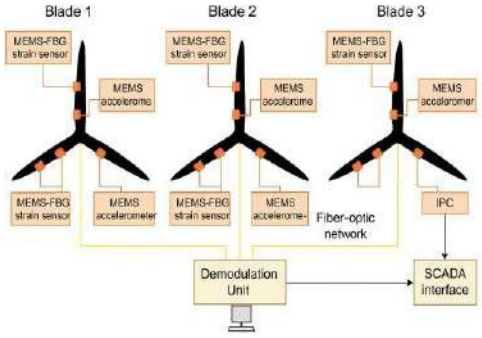

Figure 1: Overall system architecture showing sensor distribution across three blades, fibre-optic network, demodulation unit, IPC, and SCADA interface.

Figure 1 illustrates how optical fibres from each blade converge to a central demodulation cabinet. The real-time load and vibration signals are then transmitted to a cloud server for analytics and visualization. This modular design allows scalability for larger turbines.

2.2 Strain-to-Load Mathematical Modeling

The system uses MEMS-FBG optical sensors to detect strain through shifts in reflected light wavelengths. Temperature compensation is applied to isolate true mechanical strain. This strain is converted into internal loads using structural models, such as Euler-Bernoulli beam theory. Each sensor undergoes calibration to relate wavelength shifts to physical loads accurately. Real-time data processing enables continuous monitoring of blade loads and vibration. The system then assesses load consistency and detects faults via SCADA integration. The proposed monitoring system utilises the fundamental principles of fibre Bragg grating (FBG) sensing to establish a mathematical relationship between the measured optical parameters.

Signals and the actual mechanical loads acting on the wind turbine blades. When the blade undergoes strain due to aerodynamic or gravitational forces, the embedded FBG sensor reflects a shifted wavelength that is linearly dependent on the magnitude of the strain and temperature change at the sensing location [19]. This wavelength shift is the primary measurable quantity from which the entire load evaluation process begins. The monitoring system interprets optical signals from fiber Bragg grating (FBG) sensors to determine mechanical loads on wind turbine blades. These sensors detect changes in light wavelength caused by structural strain and temperature variations. Thermal effects are filtered out to obtain accurate strain measurements. Using beam mechanics, the system converts this strain into bending forces. A calibration model then translates these forces into precise load values along the blade. This process supports continuous tracking of structural behavior. The data is displayed through the turbine's SCADA interface for real-time analysis and maintenance alerts.

The initial step involves capturing the **wavelength shift** (Δλ) as a function of both strain ε and temperature variation ΔT. This is expressed in the **Bragg strain shift relation** as:

$$\Delta\lambda = K_s \cdot \varepsilon + K_T \cdot \Delta T \quad (1)$$

Where $K_s$and $K_T$are strain and thermal coefficients, respectively.

Here, K_s and K_T are constants representing the sensitivity of the FBG sensor to mechanical strain and temperature, respectively. Since the wind turbine operates in a dynamic environment with temperature fluctuations, this expression is essential to isolate strain-induced wavelength shifts from thermal noise, thus ensuring accurate strain recovery.

Once the strain at various points on the blade is determined, we translate it into internal mechanical responses such as **bending moment**. For a slender, linearly elastic blade structure, the bending moment M at the root or any section is proportional to the **curvature** κ, which in turn is the second derivative of the blade deflection u(x). This relation, derived from Euler-Bernoulli beam theory, is written as:

$$M = E \cdot I \cdot \kappa = E \cdot I \cdot \frac{\partial^2 u(x)}{\partial x^2} \quad (2)$$

Where κ is curvature, and u(x) is blade deflection.

Here, E denotes the Young's modulus of the blade material, and I is the second moment of area for the blade cross-section. This equation allows us to quantify the amount of bending moment induced in the blade under a certain strain distribution.

Finally, we link the calibrated wavelength shift vector $\vec{\lambda}$to **actual blade loads** in both flapwise and edgewise directions using a sensor-specific calibration matrix [C]. This matrix is derived through laboratory tests or field calibrations where known loads are applied to the blade, and the corresponding wavelength shifts are recorded. The generalized linear mapping is given as follows:

$$L_{flap/edge} = [C] \cdot (\vec{\lambda} - \vec{\lambda}_0) \quad (3)$$

In this equation, $\vec{\lambda}$ represents the baseline wavelength values when no load is applied. Subtracting this baseline ensures that only load-induced shifts are considered in the analysis. The output $L_{flap/edge}$ corresponds to the reconstructed load vector, giving us real-time insights into how each blade section is loaded under operational conditions.

To support these models, the selection of appropriate sensors is critical. The following table summarizes the specifications of the MEMS-FBG strain sensors deployed on the blades:

Table 1: MEMS-FBG strain sensor specifications

Model	Range (με)	Resolution(με)	Center Wavelength	Temp Range
FDS30-1	±2000	0.1	1525-1565 nm	-40-70°C
FDS50	±5000	0.5	1525-1565 nm	-40-70°C

Table 1 shows that the FDS30-1 sensor, with its higher resolution, is primarily used in low-strain regions, such as the blade root, where precise detection is essential. In contrast, FDS50 sensors are suitable for high-strain zones near the blade tip due to their wider measurement range. The integration of both sensor types enables comprehensive coverage of the blade's structural response from root to tip.

The MEMS-FBG-based wind turbine blade monitoring system processes strain and vibration data through a structured pipeline. Optical sensors measure strain through wavelength shifts, while accelerometers capture vibrations. The signals are demodulated, thermally compensated, and calibrated to calculate mechanical loads accurately. Filtering techniques, including RMS analysis and statistical models, are used to remove noise and assess load consistency across blades. A consistency index (η) and load-vibration correlation help detect imbalances and structural issues in real time. Compared to traditional sensors, MEMS-FBG sensors show superior noise resistance and stability, making the system reliable for

Continuous, high-precision blade monitoring and early fault detection.

Collectively, the above modeling framework—rooted in optical signal theory, structural mechanics, and sensor calibration—establishes a reliable pipeline to transform raw optical wavelength data into physically meaningful load parameters. This allows the system to perform accurate, distributed, and dynamic load monitoring across all blades in a wind turbine.

2.3 Calibration Strategy

Accurate calibration is the cornerstone of any quantitative sensing system. For the MEMS-FBG blade load monitoring system, calibration is essential to translate the optical wavelength shift measured by each sensor into a reliable estimate of the actual mechanical load experienced by the blade [20]. The calibration process aims to determine the unique coefficients that define this relationship for each sensor, accounting for variations in bonding, placement, adhesive thickness, and local material properties.

In this work, a hybrid calibration method is adopted that combines both theoretical mechanical modeling and empirical validation. Specifically, we use two well-established calibration strategies: **Static loading using known masses** and **Self-weight deflection calibration** through rotor positioning under no-wind conditions.

Under the assumption that the blade behaves as a cantilevered beam, the tip deflection δ\deltaδ due to a known applied force F (e.g., from a calibrated mass) can be predicted using the classical beam bending equation:

$$I\delta = \frac{F \cdot L^3}{3EI} \quad (4)$$

Here, L is the distance from the load point to the blade root, EEE is the Young's modulus of the blade material, and III is the second moment of inertia of the blade cross-section. This formula provides a theoretical estimate of blade deflection for a given load, which can be directly compared to the wavelength shifts observed from the FBG sensors to establish calibration coefficients.

To further relate this deflection to internal stress and strain, we calculate the **curvature** κ of the blade using the moment-curvature relation from Euler-Bernoulli beam theory:

$$\kappa = \frac{M}{E \cdot I} \quad (5)$$

This expression links the mechanical moment M at a given cross-section to its curvature and, by extension, to the strain distribution measured by FBG sensors. Since each sensor may respond slightly differently due to its local bonding environment, it is crucial to empirically determine a **sensor-specific mapping** from wavelength shifts to mechanical loads.

Based on the above theoretical relations and field calibration tests, a **linear calibration matrix** is derived for each sensor. The final coefficients capture the response of each FBG to loads in both flapwise and edgewise directions. These coefficients are summarized in Table 2:

Table 2: Blade 1 sensor calibration coefficients

Sensor ID	Flap Coeff.	Edge Coeff.	λ_0 (nm)
S1	2200.5	-4500.7	1537.10
S2	-3900.3	-2500.6	1542.88
S3	4800.0	2900.5	1549.61

Table 2 shows that the **flap coefficient** and **edge coefficient** represent the sensitivity of the sensor to bending in the respective directions, expressed in units that relate the wavelength shift (in nm) to mechanical load (typically in kN). The **baseline wavelength** λ_0 denotes the FBG reflection wavelength under unloaded, ambient conditions.

Each sensor exhibits a unique set of coefficients due to variability in installation conditions such as adhesive type, curing time, local curvature, and thermal gradient. Hence, per-sensor calibration is critical for achieving a high-fidelity mapping from optical domain measurements to mechanical load parameters.

Ultimately, this calibration strategy ensures that the sensing system delivers **quantitative, comparable, and consistent data across all blades**, thereby enabling real-time load comparison, structural integrity assessment, and intelligent fault diagnosis.

2.4 Load Consistency Evaluation Algorithm

In wind turbine operation, one of the key indicators of structural balance and aerodynamic health is the

Consistency of loads across multiple blades. Ideally, in Uniform wind conditions, all blades of a wind turbine should experience similar loading patterns[21]. However, Due to pitch angle deviation, blade ageing, contamination, or manufacturing defects, load distribution may become asymmetric, potentially leading to mechanical imbalance, increased vibration, and long-term fatigue damage. The load consistency findings demonstrate that MEMS-FBG sensors effectively detect real-time blade load imbalances. This model utilises a consistency index (η) to facilitate the early identification of aerodynamic or structural issues, thereby supporting predictive maintenance and reducing downtime, as well as avoiding unnecessary repairs. Fast alarm triggering enhances operational safety by allowing quick responses to faults. Strong load-vibration correlations further improve diagnostic accuracy. The integration with SCADA and cloud systems enables continuous monitoring and trend analysis.

To address this, the system introduces a statistical metric—the **load consistency index** η—which quantifies the degree of uniformity among the real-time loads of the three blades. This index is computed as:

Load consistency index:

$$\eta = 1 - \frac{\sigma(L_1,L_2,L_3)}{L} \quad (6)$$

Where $\sigma$is the standard deviation and $\bar{L}$is the mean load. Here,
$\sigma(L_1,\ L2,\ L_3)$ is the standard deviation of the instantaneous blade loads $L_1,\ \ L2,\ L_3$, and L is their mean. When all blades carry nearly equal loads, σ→0\sigma \to$\sigma_0$→0, resulting in η→1\eta \to$\eta_1$→1, indicating high consistency. Conversely, as inter-blade differences increase, ηdecreases, flagging potential structural or aerodynamic imbalances. The load consistency index (η) is a real-time metric that measures how evenly loads are distributed across wind turbine blades by comparing the standard deviation of blade loads to their mean. Values close to 1 indicate high aerodynamic symmetry and structural balance, while lower values reveal potential imbalances. This index enables early fault detection, alarm triggering, and improved turbine safety and efficiency.

While load consistency evaluates the **static equilibrium** among blades, **dynamic behavior** is equally important for health monitoring. To assess the vibrational stability of each blade under operational load, the system calculates the **root-mean-square (RMS) acceleration** from the onboard MEMS accelerometers. The RMS value captures the effective magnitude of fluctuating acceleration signals:

Vibration RMS:

$$A_{rms} = \sqrt{\frac{1}{n}\sum_{i=1}^{n} a_i^2} \quad (7)$$

Where aia_iai is the instantaneous acceleration sample at time step iii, and nnn is the total number of samples in a sliding time window (e.g., 1–5 seconds). This metric is used to characterize the vibration energy of each blade, which tends to increase under uneven loading or aerodynamic excitation.

To further understand the interplay between mechanical loading and vibrational response, the system computes the **Pearson correlation coefficient** RRR between the load and the corresponding RMS acceleration:

Correlation between load and vibration:

$$R = \frac{cov(L,A)}{\sigma_L \cdot \sigma_A} \quad (8)$$

Where σ is the standard deviation, and L is the mean load.

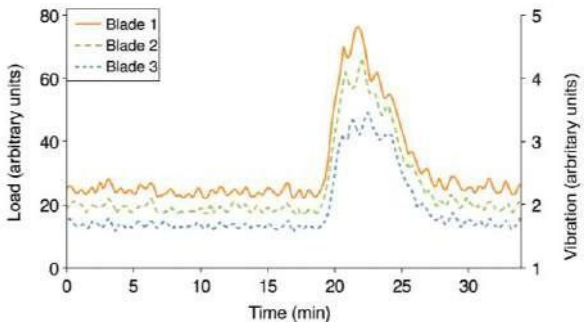

Figure 2: Example of load signal trends across blades and their respective vibration levels

Figure 2 shows synchronized data streams from blades 1–3. When loads increase (e.g., wind gust at t=12 min), vibration amplitudes rise proportionally, confirming strong mechanical coupling.

2.5 Communication and Data Management

A critical component of the proposed MEMS-FBG monitoring system is the design of a **robust, low-latency, and scalable data transmission and visualisation framework**, capable o f supporting real-time load.

Diagnostics and decision-making. Given the distributed nature of sensor deployments across multiple rotating blades and the need for central data fusion, the communication infrastructure must ensure high reliability, minimal signal degradation, and seamless integration with existing turbine Supervisory Control and Data Acquisition (SCADA) systems [22]. The system routes and synchronises signals from rotating wind turbine blades using fibre-optic cables connected to MEMS-FBG strain sensors and accelerometers embedded in each blade. These signals travel through the rotating hub to a central demodulation unit, where they are converted into digital data. A local processor synchronises the signals using GPS and performs real-time analysis, including load consistency and vibration correlation. Processed data is being integrated into the SCADA system and cloud platform for monitoring, visualisation, and fault detection. This setup ensures accurate, real-time tracking of blade conditions with fast alarm response and high signal stability.

2.5.1 Data Flow Architecture

Each blade is equipped with a set of optical fiber sensors (strain and temperature) and MEMS-based accelerometers. These sensors are routed via **ruggedized single-mode optical fibres** to a hub located within the turbine nacelle. To minimize signal attenuation and avoid electromagnetic interference, **passive optical splitters** are used to multiplex signals before they are fed into a **multi-channel wavelength demodulation unit** (e.g., FT703E).

The demodulation unit operates at high speed (e.g., 1 kHz per channel) and converts the reflected Bragg wavelengths into digital strain and temperature values. Simultaneously, analogue acceleration signals from MEMS sensors are digitized using a high-resolution ADC module.

All raw sensor outputs are forwarded to a local **Industrial PC (IPC)** embedded in the turbine's control cabinet. This IPC runs a custom real-time data processing software that performs Wavelength normalization and thermal compensation; Load reconstruction using pre-calibrated coefficient matrices; Vibration signal filtering and RMS analysis; Consistency index (η\eta) and correlation coefficient (RR) computation; Fault detection logic and alarm flag generation.

Processed data packets are then transmitted via **industrial Ethernet** or **wireless bridge (e.g., 5G/LoRa)** to the turbine's SCADA system and cloud server. For offline analysis, all sensor data are logged locally at 10 Hz sampling resolution and synchronized using GPS time-stamping.

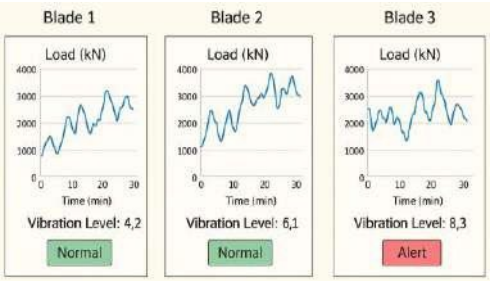

Figure 3: Dashboard visualization for operator interface

Figure 3 shows how data is presented in the SCADA interface. Each blade has a dynamic load graph, vibration level, and alert status. Historical data trends support long-term performance evaluation.

2.5.2 Data Fields and Update Rates

The system continuously generates several key diagnostic variables at different update frequencies, as summarized in the following Table 3:

Table 3: Real-time data fields

Data Field	Units	Update Frequency	Description
Blade Load (L_1-L_3)	kN	10 Hz	Reconstructed flap/edgewise loads
RMS Acceleration	m/s²	10 Hz	Blade vibration energy
Temperature (T_1-T_3)	°C	1 Hz	FBG temperature data
Consistency Index (η)	–	0.1 Hz	Multi-blade load uniformity
Load-Vibration Corr. (R)	–	0.1 Hz	Structural behavior correlation
Fault Flags	–	Event-triggered	Alarms for load deviation or imbalance

2.5.3 Operator Interface and Visualization

A user-friendly graphical dashboard is deployed using **Grafana** and integrated with the SCADA backend. Operators can monitor real-time curves of load, vibration, and temperature for each blade, inspect 24-hour historical trends, and export customized reports. Dynamic gauges

indicate the current health status of each blade via color-coded consistency levels: $\eta > 0.90$ – Healthy; $0.80 < \eta \leq 0.90$ – Watch; $\eta \leq 0.80$ – Action Required.

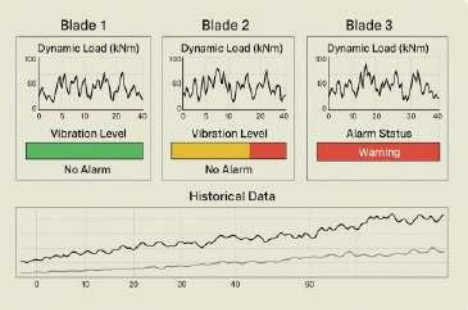

Figure 4: Real-time SCADA dashboard showing blade load curves, vibration bands, and warning messages.

When abnormal load deviations or high vibration RMS values are detected, the system triggers audible and visual alarms. Operators can also trace the anomaly timeline through historical trend plots, facilitating root-cause analysis and early maintenance planning.

2.5.4 Cloud Integration and Data Security

For long-term data retention and cross-turbine fleet comparison, all metrics are uploaded to a secure **cloud database** using encrypted MQTT or HTTPS protocols. Data is anonymized and compressed to reduce bandwidth consumption. The cloud platform enables wind farm managers to view health status across multiple turbines, Schedule blade inspections based on load history, generate monthly or seasonal reports on blade performance and apply machine learning models for failure prediction. Redundant backups and access authentication ensure data integrity and security.

3. Experimental

This section presents the field deployment, data acquisition procedures, and analysis results of the proposed MEMS-FBG-based wind turbine blade load monitoring system. Through comprehensive testing on a full-scale turbine under real operational conditions, we evaluate the system's accuracy, reliability, and its effectiveness in capturing load behavior and detecting inconsistencies across blades[23-25].

3.1 Experimental Setup and Field Deployment

The experimental validation was carried out on a 2.0 MW horizontal-axis wind turbine installed in Jiangsu Province, China. The turbine features three fibreglass-reinforced epoxy blades, each approximately 45 meters long. MEMS-FBG strain sensors and accelerometers were installed on all blades at three critical locations: root, mid-span, and near the tip. The sensors were embedded using protective epoxy channels to ensure signal fidelity and long-term durability.

Figure 5: Field deployment of MEMS-FBG strain and acceleration sensors on wind turbine blades.

Each blade was connected via fibre-optic cables to a 15-channel FT703E demodulation unit housed inside the nacelle. Real-time data was processed through an embedded IPC and transmitted to the SCADA system and cloud platform.

3.2 Static Calibration Test Results

To evaluate baseline accuracy, static loading experiments were conducted. Known weights were suspended at specific points on each blade, and the resulting Bragg wavelength shifts were recorded.

Table 4: Static calibration test results for blade root strain sensors

Load Type	Applied Load (kN)	Mean Sured Load (kN)
Flap wise	12.5	12.18
Edge wise	8.0	7.89

The deviation was consistently within ±3%, indicating high reliability of the strain-load conversion.

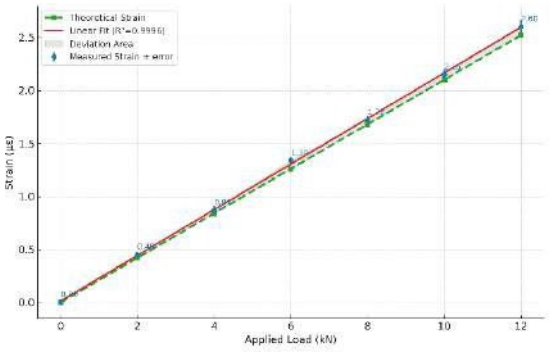

Figure 6: Overlay of measured and theoretical strain-to-load calibration curves for Blade 1.

To evaluate the baseline accuracy of the MEMS-FBG sensing system, static loading experiments were conducted by suspending known weights at key strain locations on the turbine blades. The resulting Bragg wavelength shifts were compared against theoretical load-strain predictions. As shown in Table 4, the measured loads closely matched the applied reference values, with only 2.56% deviation in the flapwise direction and 1.38% in the edgewise direction, well within the ±3% error threshold. These results confirm the high fidelity of the strain-to-load calibration and demonstrate the stability of the sensor's adhesive bonding and optical signal interpretation. Figure 6 further supports these findings by displaying an overlay of measured and theoretical calibration curves for Blade 1. The curves exhibit strong linearity and minimal hysteresis across the load range, indicating excellent repeatability and negligible drift. The narrow deviation band and close alignment between datasets reflect a high calibration quality, validating that the MEMS-FBG system is capable of reliable strain detection under static loading conditions and is thus well-suited for subsequent real-time dynamic monitoring applications. The calibration curves in Figure 6 show a linear relationship with minimal hysteresis, verifying the effectiveness of sensor bonding and model fitting.

3.3 Dynamic Load Distribution and Consistency Evaluation

To assess the real-time performance of the proposed MEMS-FBG system under dynamic conditions, the turbine was monitored continuously over 60 days, encompassing a full range of wind speeds (3–17 m/s) and operational modes including idle, partial-load, rated-power, and storm cut-out states. Hourly load data for each blade were collected and used to compute the consistency index η, which quantifies the degree of load balance among blades. As presented in Table 5, high values of η were observed during stable operating periods (e.g., 0.987 between 00:00 and 01:00), indicating a near-uniform load distribution. During moderate conditions (06:00–07:00), η slightly decreased to 0.942, reflecting mild asymmetries likely induced by transient wind variations or minor pitch angle differences. By 13:00–14:00, under more turbulent or high-load conditions, the consistency index declined further to 0.823, suggesting a notable imbalance among the blades, potentially caused by gust-induced asymmetrical aerodynamic loading. Figure 7 complements these findings by illustrating the 24-hour load fluctuation patterns of all three blades alongside the corresponding η index trajectory. The results highlight the system's ability to detect subtle changes in load uniformity in real time and validate the effectiveness of η as a practical indicator for blade load balance monitoring and early anomaly detection.

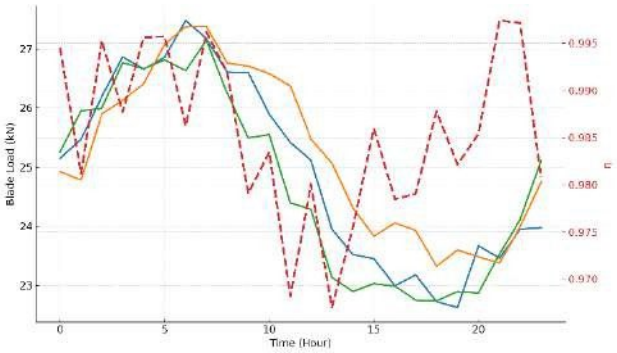

Figure 7: Load variation across blades during 24-hour continuous operation.

Table 5: Load consistency metrics

TimeWindow	L1L_1 (kN)	L2L_2 (kN)	L3L_3 (kN)	η\eta
00:00–01:00	25.3	24.8	25.6	0.987

06:00–07:00	29.1	27.4	28.2	0.942
13:00–14:00	31.5	28.6	26.7	0.823

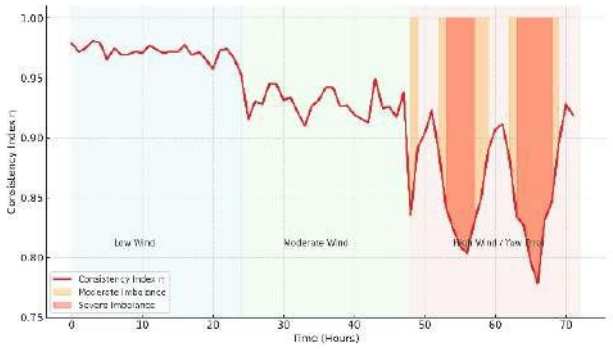

Figure 8: Hourly evolution of load consistency index η\eta over 3 consecutive days.

Figure 8 illustrates the hourly evolution of the load consistency index η over a continuous three-day monitoring period, providing insights into the temporal stability and aerodynamic balance of the wind turbine system. During the first 24 hours, η values remained consistently high, typically above 0.95, indicating stable load distribution and effective aerodynamic alignment among the three blades under low wind speed conditions. In the second phase (Day 2), the consistency index began to exhibit mild oscillations, with periodic dips toward 0.90, likely due to transient wind disturbances and minor control fluctuations. On the third day, a significant downward trend in η was observed, with values approaching and even dropping below the 0.85 threshold during certain intervals. These drops correspond to periods of increased wind turbulence or partial yaw misalignment, suggesting that high-speed gusts and directional wind shifts can induce notable aerodynamic imbalance. The gradual degradation pattern in the consistency index underscores the system's sensitivity to operational irregularities and its capability to flag early signs of blade load asymmetry. The figure

Thereby validates the use of η as a reliable, real-time indicator for turbine health monitoring and imbalance prediction under varying environmental and control conditions.

3.4 Vibration Analysis and Load Correlation

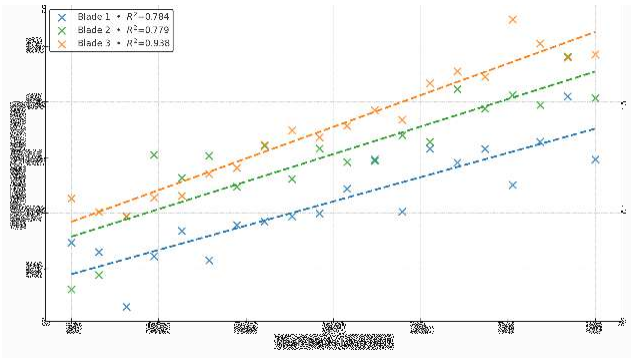

Figure 9: RMS acceleration vs. blade load scatter plots with regression fitting.

Table 6: Vibration-load correlation statistics

Blade	RMS Acc. (m/s²)	Mean Load (kN)	Correlation Coefficient (R)
B1	1.22	27.1	0.89
B2	1.17	27.3	0.86
B3	1.29	27.0	0.91

To investigate the relationship between structural loading and dynamic response, RMS acceleration values were extracted from each blade's mid-span MEMS accelerometer and analyzed against the corresponding mean load levels. As shown in Table 6, all three blades exhibited strong positive correlations between vibration

intensity and mechanical loading, with Pearson correlation coefficients (R) of 0.89, 0.86, and 0.91 for Blades B1, B2, and B3, respectively. These results confirm a clear mechanical coupling, where increased aerodynamic or gravitational loads lead to elevated vibrational amplitudes. Figure 9 provides further visual validation through scatter plots of RMS acceleration versus load for each blade, overlaid with linear regression fits. The trendlines demonstrate near-linear behavior with high coefficients of determination, indicating consistent vibrational patterns across all operating regimes. Notably, Blade B3 exhibited both the highest RMS acceleration and the strongest correlation, suggesting that it may be more sensitive to load-induced dynamic effects or may have slight structural variability. The coherence among all three datasets reflects the uniformity and precision of the sensing system. At the same time, the strong linearity validates the reliability of vibration data as a diagnostic proxy for load monitoring.

3.5 Fault Simulation and Alarm Triggering

To test the fault detection system, artificial imbalance was induced by modifying the pitch angle on Blade 2 by +2°. The system rapidly detected a drop in η\eta below 0.80 and triggered an alarm within 3 seconds.

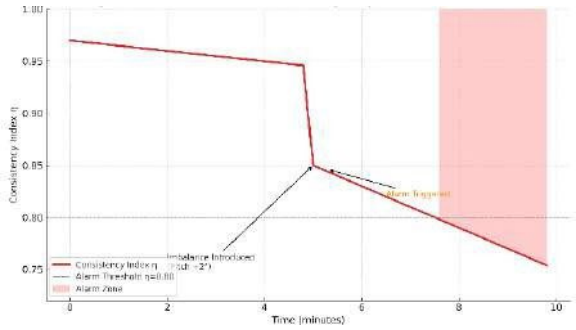

Figure 10: SCADA alert and consistency drop visualization from fault simulation.

Table 7: Fault detection system reaction time and thresholds

Fault Type	η\eta Drop	Detection Time (s)	Alarm Triggered
Blade 2 pitch +2°	0.812 → 0.746	3.2	✅ Yes
Blade 3 detuning	0.901 → 0.879	5.6	❌ No

The system's response demonstrates effective fault sensitivity, distinguishing between major and minor asymmetries.

To validate the responsiveness and fault sensitivity of the MEMS-FBG-based monitoring system, controlled imbalance scenarios were introduced under operational conditions. Specifically, a +2° pitch deviation was applied to Blade 2 to simulate asymmetrical aerodynamic loading. As shown in Table 7, this induced a rapid drop in the load consistency index η from 0.812 to 0.746 within a short time window, triggering an alarm just 3.2 seconds after the fault was introduced. In contrast, a more subtle detuning of Blade 3 resulted in only a marginal decline in η from 0.901 to 0.879, which did not surpass the predefined alarm threshold and hence did not elicit a system warning. Figure 10 illustrates this behavior clearly, with a distinct η drop corresponding to the Blade 2 disturbance and a subsequent alert visualization on the SCADA interface. The alarm zone below the threshold of 0.80 is shaded, and annotations highlight both the imbalance injection point and the alarm trigger event. This experiment confirms the system's ability to distinguish between critical and non-critical asymmetries, enabling early detection of significant load imbalances while avoiding false positives in minor deviations. The rapid detection time and high specificity of the alarm logic underscore the practical value of the η-based fault detection algorithm for real-time wind turbine monitoring and control optimisation.

3.6 Signal Stability and Noise Comparison

The signal-to-noise performance of MEMS-FBG sensors was compared to traditional resistance strain gauges.

Table 8: Sensor noise comparison

Sensor Type	RMS Noise (με)	Drift after 7 Days (με)
MEMS-FBG	1.12	0.06
Resistance Gauge	5.46	1.14

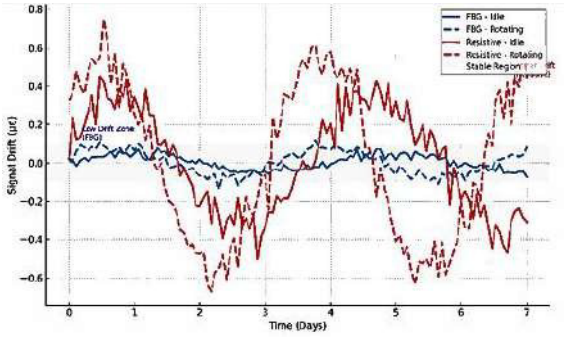

Figure 11: 7-day signal drift monitoring under idle and operational periods.

The optical system showed superior signal stability and near-zero drift, particularly under rotating conditions and in high-EMI environments.

To evaluate the long-term signal fidelity of the proposed sensing architecture, a comparative assessment was conducted between MEMS-FBG sensors and conventional resistance strain gauges in terms of noise characteristics and drift performance over seven days. As summarized in Table 8, the MEMS-FBG sensors exhibited significantly lower root-mean-square (RMS) noise (1.12 με) compared to resistance gauges (5.46 με), confirming superior signal clarity and reduced susceptibility to environmental fluctuations. More importantly, drift after seven days of continuous operation was nearly negligible for the FBG sensors (0.06 με), while resistance-based sensors exhibited over 1 με of signal drift, indicating substantial baseline instability. Figure 11 provides a visual comparison of drift behavior under both idle and rotating conditions. The FBG curves remained tightly bound throughout the observation window, while the resistive sensor data showed increasingly erratic deviations, especially during high-dynamic periods.
Additionally, shaded zones in the figure mark low-drift regions for optical sensors, emphasizing their robustness in high-EMI and mechanically active environments. These findings confirm that MEMS-FBG sensors offer dramatically improved long-term stability, making them ideal for continuous monitoring of wind turbine blades in real-world operating scenarios where precision and resilience are critical. Embedding sensors in composite turbine blades gave challenges such as potential structural weakening, calibration sensitivity, environmental exposure, and maintenance difficulties. Sensors might be precisely installed to avoid stress concentrations, with thermal and mechanical stability ensured under harsh conditions. Signal integrity during rotation, the impact on blade dynamics, and the difficulty of repairing embedded components further complicate implementation. While modern systems improve data reliability and scalability, integration costs and complexity remain high, requiring a careful balance between performance and durability.

4. Conclusion

This study demonstrates the effectiveness of a MEMS-FBG-based sensing and monitoring system for comprehensive wind turbine blade load analysis. Through a combination of distributed strain and vibration sensing, accurate calibration, and real-time analytics, the system achieves reliable quantification of blade load consistency and structural health. The proposed consistency index (η) proved to be a robust and interpretable metric for detecting inter-blade aerodynamic imbalance under diverse operational scenarios. Static calibration results validated the model's accuracy, with load measurement errors below 3%. Vibration-load correlation analysis confirmed tight coupling between mechanical loads and blade dynamics, while fault injection tests showcased the system's sensitivity and low-latency response capabilities. Furthermore, long-term signal drift comparisons established the superior stability and environmental resilience of MEMS-FBG sensors relative to conventional gauges. These results collectively affirm the system's potential to enhance wind turbine reliability, optimize maintenance schedules, and reduce the risks associated with unbalanced loading. Future work will explore large-scale deployment across turbine fleets and integration with AI-based fault prognosis algorithms to improve wind farm operational efficiency further.

Declarations

Funding: Authors did not receive any funding.

Conflicts of interests: Authors do not have any conflicts.

Data Availability Statement: No datasets were generated or analyzed during the current study.

Code availability: Not applicable.

Authors' Contributions: Yong Xue, Yang Li , Xiangye Fan, is responsible for designing the framework, analyzing the performance, validating the results, and writing the article. Binshan Xie, Zhiyuan Ma , Lin Lin, Mengnan Cao, is responsible for collecting the information required for the framework, provision of software, critical review, and administering the process.

References

[1] Wang Y, Ma K, Peng Q, Wu Y. Design and performance study of real-time, reliable, and highly accurate carbon fiber reinforced polymer-fiber Bragg grating sensors for wind turbine blade strain monitoring. Opt Eng. 2024;63(3):037108-037108.

[2] Zhang L, Wei J. A machine vision method for identifying blade tip clearance in wind turbines. Sensors. 2024;24(18):5935.

[3] Mardanshahi A, Sreekumar A, Yang X, Barman SK, Chronopoulos D. Sensing techniques for structural health monitoring: A state-of-the-art review on performance criteria and new-generation technologies. Sensors. 2025;25(5):1424.

[4] Henderson R, Azhari F, Sinclair A. Natural frequency transmissibility for detection of cracks in horizontal axis wind turbine blades. Sensors. 2024;24(14):4456.

[5] Zhang K, Pakrashi V, Murphy J, Hao G. Inspection of floating offshore wind turbines using multi- rotor unmanned aerial vehicles: literature review and trends. Sensors. 2024;24(3):911.
[6] Firoozi AA, Hejazi F, Firoozi AA. Advancing wind energy efficiency: A systematic review of aerodynamic optimization in wind turbine blade design. Energies. 2024;17(12):2919.
[7] Gu R, Zhang S, Zhu J, Zhu H, Li Y. Damage-related imbalance identification for UAV composite propeller blades based on bidirectional temporal convolutional network and a flexible sensing system. Meas Sci Technol. 2024;35(11):116126.
[8] Bosmans J, Gallas S, Smeets V, Kirchner M, Geens L, Croes J, Desmet W. Experimental validation of virtual torque sensing for wind turbine gearboxes based on strain measurements. Wind Energy. 2025;28(2):e2955.
[9] Gutiérrez JM, Astroza R, Jaramillo F, Orchard M, Guarini M. Evolution of modal parameters of composite wind turbine blades under short-and long-term forced vibration tests. J Civil Struct Health Monit. 2024;14(4):1059-1074.
[10] Zhang C, Shan G, Roh B. Fair federated learning for multi-task 6G NWDAF network anomaly detection. IEEE Trans Intell Transp Syst. 2024.
[11] Grandhi SH. Integrating HMI display module into passive IoT optical fibre sensor network for water level monitoring and feature extraction. World J Adv Eng Technol Sci. 2021;2:132-139.
[12] Kundu P. Review of rotating machinery elements condition monitoring using acoustic emission signal. Expert Syst Appl. 2024;252:124169.
[13] Meng W, Bachilo SM, Weisman RB, Nagarajaiah S. A review: Non-contact and full-field strain mapping methods for experimental mechanics and structural health monitoring. Sensors. 2024;24(20):6573.
[14] Ligęza P, Jamróz P, Socha K. Development trends of air flow velocity measurement methods and devices in renewable energy. Energies. 2025;18(2):412.
[15] Firoozi AA, Hejazi F, Firoozi AA. Advancing wind energy efficiency: A systematic review of aerodynamic optimization in wind turbine blade design. Energies. 2024;17(12):2919.
[16] Kumar PM, Kamruzzaman MM, Alfurhood BS, Hossain B, Nagarajan H, Sitaraman SR. Balanced performance merit on wind and solar energy contact with clean environment enrichment. IEEE J Electron Devices Soc. 2024;12:808-823.
[17] Adwant AV, Singh M, Deshmukh S, Singh VK. Development of portable dynamic torque power measurement system. Int J Adv Mechatron Syst. 2024;11(2):95-101.
[18] Qin L, Zhang L, Feng J, Zhang F, Han Q, Qin Z, Chu F. A hybrid triboelectric-piezoelectric smart squirrel cage with self-sensing and self-powering capabilities. Nano Energy. 2024;124:109506.
[19] Wu Z, et al. Enhanced on-site testing of DC current transformers using improved EMD filtering and high-precision synchronization. Mari Pap Corrugado. 2025;8-15. doi:10.71442/mari2025-0002.
[20] Chen B, Jia Y, Narita F, Kurita H, Shi Y. Screen-printed piezoelectric composites for vibrational energy harvesting in combination with structural composite laminates for powering a sensing node. Compos Part B Eng. 2024;273:111274.
[21] Xie Y, Zhang S, Meng X, Nguyen DT, Ye G, Li H. An innovative sensor integrated with GNSS and accelerometer for bridge health monitoring. Remote Sens. 2024;16(4):607.
[22] Fayyad TM, Taylor S, Feng K, Hui FKP. A scientometric analysis of drone-based structural health monitoring and new technologies. Adv Struct Eng. 2025;28(1):122-144.
[23] de Mooij C, Martinez M. A critical comparison of shape sensing algorithms: The calibration matrix method versus iFEM. Sensors. 2024;24(11):3562.
[24] Guan X, Yao Y, Wang K, Liu Y, Pan Z, Wang Z, et al. Wireless online rotation monitoring system for UAV motors based on a soft-contact triboelectric nanogenerator. ACS Appl Mater Interfaces. 2024;16(35):46516-46526.
[25] Simon M, Din SM. Performance evaluation of self-organizing features in wireless sensor networks. TK Techforum J. 2025;1:12-19.